PNAS RESEARCH ARTICLE | BIOPHYSICS AND COMPUTATIONAL BIOLOGY

A minimal physical model for curvotaxis driven by curved protein complexes at the cell's leading edge

Raj Kumar Sadhu[a,1,2], Marine Luciano[b,c], Wang Xi[d], Cristina Martinez-Torres[e], Marcel Schröder[f], Christoph Blum[f], Marco Tarantola[f], Stefano Villa[f], Samo Penič[g], Aleš Iglič[g], Carsten Beta[e,h], Oliver Steinbock[i], Eberhard Bodenschatz[f], Benoît Ladoux[d], Sylvain Gabriele[c], and Nir S. Gov[a,2]

Edited by Pascal Silberzan, Institut Curie, Paris, France; received April 27, 2023; accepted January 29, 2024 by Editorial Board Member Herbert Levine

Cells often migrate on curved surfaces inside the body, such as curved tissues, blood vessels, or highly curved protrusions of other cells. Recent in vitro experiments provide clear evidence that motile cells are affected by the curvature of the substrate on which they migrate, preferring certain curvatures to others, termed "curvotaxis." The origin and underlying mechanism that gives rise to this curvature sensitivity are not well understood. Here, we employ a "minimal cell" model which is composed of a vesicle that contains curved membrane protein complexes, that exert protrusive forces on the membrane (representing the pressure due to actin polymerization). This minimal-cell model gives rise to spontaneous emergence of a motile phenotype, driven by a lamellipodia-like leading edge. By systematically screening the behavior of this model on different types of curved substrates (sinusoidal, cylinder, and tube), we show that minimal ingredients and energy terms capture the experimental data. The model recovers the observed migration on the sinusoidal substrate, where cells move along the grooves (minima), while avoiding motion along the ridges. In addition, the model predicts the tendency of cells to migrate circumferentially on convex substrates and axially on concave ones. Both of these predictions are verified experimentally, on several cell types. Altogether, our results identify the minimization of membrane-substrate adhesion energy and binding energy between the membrane protein complexes as key players of curvotaxis in cell migration.

curvotaxis | cell migration | curved surfaces | membrane proteins

Significance

How cells migrate when exposed to curvature cues (curvotaxis), is important for understanding cell migration inside complex tissues, however, the underlying mechanisms are not well understood. Here, we use a theoretical "minimal cell" model, which is formed using a closed vesicle containing curved membrane proteins coupled with active (cytoskeleton) forces, that self-organizes to form a motile phenotype. Using this "minimal cell" model we systematically explore the curvotaxis mechanism on various curved surfaces. The model cell recovers previously observed migration patterns, and the predictions are also verified by experiments with different cell types. The simplicity of our model and the physical origin of the emergent curvotaxis make these conclusions relevant to many cell types exhibiting lamellipodia-based migration.

Cell migration is an important biological process that plays a central role in immune response, wound healing, tissue homeostasis, etc (1, 2). While the environment of a cell in vivo is geometrically complex, most of the studies focus on cell spreading and migration on flat substrates (3–5). Previous studies on two-dimensional (2D) patterned flat surfaces have shown that cells adapt their shape and their internal cytoskeleton to these 2D geometries (6–8). However, eukaryote cells, adhering and migrating on a solid substrate, are observed to also interact with the topography of the substrate and modify their motility (9–11). The alignment and the direction of migration of isolated cells, in response to the topography, crucially depends upon the cell type. For example, fibroblasts are found to align axially on the surface of a cylinder, while epithelial cells align circumferentially (12–14). In another experiment (10), the migration of T-lymphocytes was studied on a surface with sinusoidal (wavy) height undulations. The cells were found to move axially in the grooves (minima) of the surface topography, avoiding migration on the ridges (maxima). In ref. 11, the dynamics of several cell types was studied on a 2D sinusoidal surface. Adherent fibroblast cells, dominated by stress fibers and weakly motile, were found to settle in the concave grooves or adhere aligned to the undulation axis (both on grooves and ridges) (15, 16). In many adherent cells, the alignment is found to be determined by the competition between the bending energy of the stress fibers, of the nucleus and the contractile forces (17–19).

At the level of cell collectives, both alignment and cell migration within the confluent tissue are found to be affected by the substrate curvature, experimentally (20–25) and in theoretical analysis (26).

Despite these studies, the underlying mechanisms that determine the response of migrating cells to the substrate curvature are still not well understood, even at the level of single migrating cells. A few theoretical studies addressed the curvature response of an isolated motile cell. One model contains a detailed description of the cellular mechanics, and is based on the assumption of a central role for the nuclear dynamics in controlling the cell migration on the curved surface (27). A similar approach of modeling cell migration as arising from coupling the nucleus to random peripheral protrusions

The authors declare no competing interest.

This article is a PNAS Direct Submission. P.S. is a guest editor invited by the Editorial Board.

[1]Present address: Institut Curie, PSL Research University, CNRS, UMR 168, Paris 75007, France.

[2]To whom correspondence may be addressed. Email: raj-kumar.sadhu@curie.fr or nir.gov@weizmann.ac.il.

This article contains supporting information online at https://www.pnas.org/lookup/suppl/doi:10.1073/pnas.2306818121/-/DCSupplemental.

Published March 15, 2024.

(28), produced migration patterns that were in qualitative agreement with observations (10), i.e., resulting in cells migrating preferentially along the grooves. Another model provides a simpler and more general description in terms of an active-fluid (29), but its predictions were not systematically compared to experiments. A similar model was proposed to describe amoeba cells moving along ridges, guided by a reaction–diffusion mechanism adapted from macropinocytic cup formation (30). Dynamic changes in substrate curvature were also shown to guide cell migration over long distances (31).

For cell migration that is driven by the lamellipodia protrusion, understanding the migration on curved substrates requires an understanding of the mechanisms that drive the formation of the lamellipodia. Recently we have proposed a theoretical model where the lamellipodia forms as a self-organization of curved actin nucleators, coupled with adhesion to the substrate (32, 33). We showed that due to the spontaneous curvature of the actin nucleators, they aggregate at the cell-substrate contact line, and induce an outward normal force, which represents the protrusive force due to actin polymerization. Curvature-sensitive membrane complexes that contain actin nucleation factors (34–37) have been found in experimental observations at the leading edge of cellular protrusions (38–41). This model can give rise to the spontaneous formation of a lamellipodia-like protrusion, with a stable and asymmetric leading edge, that drives the migration of the simulated membrane vesicle (Fig. 1*A*). We found these motile vesicles to be highly persistent on a flat surface, maintaining robustly their direction of migration (33), resembling persistently motile cell fragments (42).

Here, we use the spontaneously migrating vesicle that arises in our model (Fig. 1), as a minimal model of a migrating cell, to explore its behavior and motility on a wide range of curved surfaces. Indeed, we explore surfaces with smooth sinusoidal shape undulations, as well as fibers (outside of cylindrical surfaces) and tubes (inside of cylinders). We do not explore here topographies with sharp edges and barriers or on length-scales much smaller than the cellular length-scale such as these experimental studies (43–45), as these will require a much finer mesh for the vesicle surface triangulation and are consequently computationally costly. In addition, sharp edges will increase the chance of our motile vesicle losing its polarity (defined as the net magnitude of the active force exerted on the vesicle surface) (33).

Despite the simplicity of our model, the migration patterns of our motile vesicle on the curved surfaces correspond closely to published, as well as recent experimental observations that we present here, of cell migration over curved surfaces. The model vesicle is found to move perpendicular to a sinusoidal topography of short length-scale, while it tends to migrate circumferentially around fibers (and pillars). These qualitative features of the calculated migration patterns of the motile vesicle, are verified by comparing to the migration patterns of several motile cell types. Our minimal model for cell migration suggests that some aspects of curvotaxis, of cells that migrate using lamellipodia protrusions, can be universally explained using physical principles.

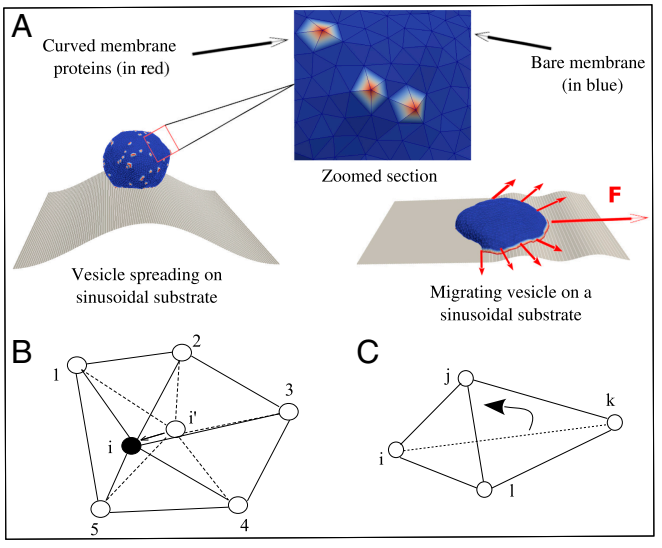

Fig. 1. Schematic representation of our model. (*A*) The vesicle is formed by a closed triangulated surface, having N vertices connected to its neighbors with bonds. These bonds can change their length such that they are never below $l_{\min}$, or above $l_{\max} = 1.7l_{\min}$. The red dots on the surface of the vesicle represent the curved membrane protein complexes with positive intrinsic curvature (convex), while the blue part represents bare membrane. A zoomed version of a small section of the vesicle surface is shown in the *Inset*. We show here two possible initial conditions: (*Left*) The vesicle starts with a spherical-like shape, adheres, spreads, and migrates on the curved surfaces. (*Right*) We generate a motile (crescent shaped) vesicle on a flat substrate and then deform the surface and let the vesicle evolve to conform to the deformed (curved) shape, and then allow it to migrate. (*B*) Vertex movement: The vertex i' is moved to i. (*C*) Bond flip: The bond $i-k$ is flipped to bond $j-l$.

1. Theoretical Model

The migrating cell is represented in our theoretical model using a three-dimensional membrane vesicle. The vesicle is described by a closed triangulated surface having N vertices, connected to their neighbors with bonds, and forming a dynamically triangulated, self-avoiding network, with the topology of a sphere (32, 33, 46–50) (Fig. 1). The nodes that compose the vesicle surface can either represent the bare membrane (blue in Fig. 1), or represent membrane protein complexes with convex spontaneous curvature (37), that diffuse on the membrane surface, having nearest-neighbor attractive interaction with each other (red in Fig. 1). Convex protein or membrane curvature stands for a node that is locally protruding outward, with respect to the vesicle interior.

We consider that each curved protein complex recruits actin polymerization, which gives rise to a local protrusive force that pushed the membrane. This is represented in our model as an active force (F) exerted at the site of the curved protein on the membrane, in the direction of the local outward normal to the vesicle surface. The simplifying assumption is that the actin polymerization that occurs near the membrane can be treated as a local force exerted directly at the site of the curved protein complex which includes actin nucleation factors such as the WAVE complex (51–53).

The vesicle energy has therefore the following contributions: The continuum version of the bending energy is given by

$$W_b = \frac{\kappa}{2}\int_A (H - H_0)^2 dA, \qquad [1]$$

where κ is the bending rigidity, H is the mean local curvature of the membrane surface, H_0 is the local spontaneous curvature, and the integral is over the entire surface. The vesicle contains curvature-sensitive protein complexes, that occupy vertices with an overall density $\rho = N_c/N$, where N_c is the number of such protein nodes that are initially randomly distributed over the vesicle surface, and their total number is kept constant throughout the simulation, and N is the total number of vertices on the vesicle. These protein nodes have a positive (convex) spontaneous curvature ($H_0 > 0$), while the bare membrane nodes have zero spontaneous curvature. In our simulations we

use a discrete version of the bending energy (54, 55) (*SI Appendix*, section S1).

The direct binding energy between the protein complexes on nearest-neighbor nodes is given by

$$W_d = -w \sum_{i<j} \mathcal{H}(r_0 - r_{ij}), \quad [2]$$

where, $\mathcal{H}$ is the Heaviside step function, $r_{ij} = |\overrightarrow{r_j} - \overrightarrow{r_i}|$ is the distance between proteins, $\overrightarrow{r_i}$, $\overrightarrow{r_j}$ are the position vectors for $i, j - th$ proteins, and r_0 is the range of attraction, w is the strength of attraction. The range of attraction is chosen such that only the proteins that are in neighboring vertices can bind to each other.

These curved protein complexes also recruit actin filaments that polymerize at the location of these proteins. We assume that the direction of these forces is normally outward of the local surface containing the proteins. The active energy is given by

$$\Delta W_F = -F\, \hat{n}_i \cdot \overrightarrow{\Delta r}_i, \quad [3]$$

where, F is the magnitude of the active force, representing the protrusive force due to actin polymerization (33, 48) that is acting in the direction of outward normal vector of the local membrane surface (along $\hat{n}_i$) and $\overrightarrow{\Delta r}_i$ is the displacement vector of the protein complex. The "active" forces in our simulations are implemented as external forces that act on the specific nodes of the system that contain the curved membrane proteins (with positive spontaneous curvature, red nodes in Fig. 1). This is done by giving a negative energy contribution when the points on which these forces act move in the direction of the force. These forces are "active" since they give an effective energy (work) term that is unbounded from below and thereby drive the system out of equilibrium. By exerting a force directed at the outward normal we naturally describe Arp2/3-driven branching polymerization of actin, which is rather isotropic and acts as a local pressure on the membrane.

Finally, the adhesion energy due to the interaction between the vesicle and the extracellular substrate is given by

$$W_A = -\sum_{i'} E_{ad}, \quad [4]$$

where E_{ad} is the adhesion energy per node, and the sum runs over all the vertices that are adhered to the substrate (32, 33, 56). By "adhered vertices," we mean all such vertices, whose perpendicular distance from the adhesive surface is less than a threshold, which we chose to be equal to the length l_{min}, which is the unit of length in our model, and defines a minimal length allowed for a bond. Thus, the total energy of the system is given by

$$W = W_b + W_d + W_F + W_A. \quad [5]$$

We update the vesicle with mainly two moves, 1) vertex displacement and 2) bond flip. In a vertex displacement, a vertex is randomly chosen and moved by a random length and direction, with the maximum possible distance restricted by 0.15 $l_{\min}$ (Fig. 1*B*). This movement provides shape fluctuations to the vesicle. In the bond flip move, a single bond is chosen, which is a common side of two neighboring triangles, and this bond is cut and reestablished between the other two unconnected vertices (Fig. 1*C*) (32, 33, 56). The bond flip is responsible for the lateral fluidity of the system that allows the vertices to diffuse through the membrane surface. Since our protein complexes are attached to a particular vertex, it also diffuses along with the vertex in the bond flip movement. The maximum bond length is restricted to $l_{\max} = 1.7\ l_{\min}$ in order to maintain self-avoidance of triangulated network. We update the system using the Metropolis algorithm, where any movement that increases the energy of the system (Eq. **5**) by an amount ΔW occurs with rate $\exp(-\Delta W/k_B T)$, otherwise it occurs with rate unity.

We chose the physical parameters of the model to be in the regime where we get a robust motile vesicle shape (as shown in Fig. 1*A*), which constrains the values of F, E_{ad} and ρ (*SI Appendix*, section S3 and Fig. S2). Specifically, we emphasize that we do not tailor our model parameters to fit specific experiments, but only maintain the model in the regime of motile vesicle shape. We then utilize this motile vesicle to explore qualitatively its behavior on different curved surfaces and compare these qualitative behaviors with the experiments.

2. Results

When simulating the migration of our motile vesicle (Fig. 1) on curved surfaces, we have to note that our motile vesicle can easily lose its polarization and motility if it encounters large amplitude and sharp height undulations or barriers (33). This "fragility" of the motile phenotype in our model constrains us to explore surfaces with small gradients of height undulations, such that our vesicle does not lose its polarization and motility. Our vesicle loses its motility when its leading edge protein cluster (Fig. 1) breaks up into two or more parts, which happens when the vesicle collides with an obstacle of large height gradient, or can occur spontaneously due to noise (33). In our model this event is irreversible, while in real cells there are internal mechanisms that allow cells to recover their polarized shape and resume motility (57–59).

We therefore explore below the migration of our motile minimal-cell system on smooth surfaces where the curvature changes gradually on the length-scale of the vesicle surface triangulation. The shape of the sinusoidal substrate in the simulation is of the form: $z = z_m \sin(2\pi y/y_m)$, such that the sinusoidal variations are along the y-direction and the curvature remains constant along the x-direction. We use several combinations of z_m and y_m in our simulations: 1) $z_m = 10\ l_{\min}$; $y_m = 120\ l_{\min}$, 2) $z_m = 2\ l_{\min}$; $y_m = 30\ l_{\min}$, and 3) $z_m = 1\ l_{\min}$; $y_m = 15\ l_{\min}$, to capture experimental observations that were performed using different ratio of the cell size and the wavelength of the sinusoidal pattern (*SI Appendix*, Fig. S3). By keeping the ratio $z_m/y_m \ll 1$, we remain in the regime of small undulations, which maintains the motility of our simulated vesicle. Similarly for the migration on fibers and inside tubes, we keep their radius large compare with the triangulation length-scale.

In the simulations with sinusoidal surface, we start with a motile vesicle, that we formed on a flat substrate, in which all the proteins are in a single cluster and exert a net force in the direction of migration. We then deform the substrate into a curved shape and allow the vesicle to evolve so that it matches the curved substrate to which it is adhered (see *SI Appendix*, section S5 and Fig. S4 and Movie S1 for more details). This allows us to control the initial direction of motion of the vesicle. Alternatively, we can start from a spherical-like vesicle and let it spread over the curved surface. During this spreading the system often breaks the symmetry spontaneously by self-organizing all the proteins in a single cluster that forms the leading edge, thereby forming a motile shape. However, in this case, we do not have any control over the initial direction of migration.

A. Cellular Migration on Sinusoidal Surfaces: Large Wavelength. We start by studying the vesicle migration on a sinusoidal substrate where the sinusoidal wavelength is larger than the diameter of the adhered cell, and the vesicle can migrate while it is roughly in a region with only one type of substrate curvature over its entire contact surface with the substrate: The groove/ridge width $y_m/2$ is about twice larger than the cell diameter $2R_{vesicle}$. In Fig. 2 *i* and *ii* we show the configurations and trajectories of a motile vesicle that was placed initially either on the *Bottom* (Fig. 2*A*) or *Top* (Fig. 2*B*) of the sinusoidal surface undulation. The vesicle is initially aligned parallel to the surface undulations (along the *x*-axis).

When we use a vesicle of small size (Fig. 2 *A* and *B*), we find simple dynamics on the sinusoidal surface: When initiated inside the groove, it maintains its aligned direction of motion (Fig. 2*A* and Movie S2). When initiated on the ridge, the vesicle quickly reorients to almost perpendicular direction of motion, slides to the nearby groove, where it resumes its aligned migration (Fig. 2*B* and Movie S3).

A larger vesicle (surface area five times larger) on the same sinusoidal substrates exhibits more complex dynamics (Fig. 2 *C* and *D*; Movies S4 and S5). This is due to the vesicle now extending over a larger surface and simultaneously spanning more of the two signs of the substrate curvatures. For example, when

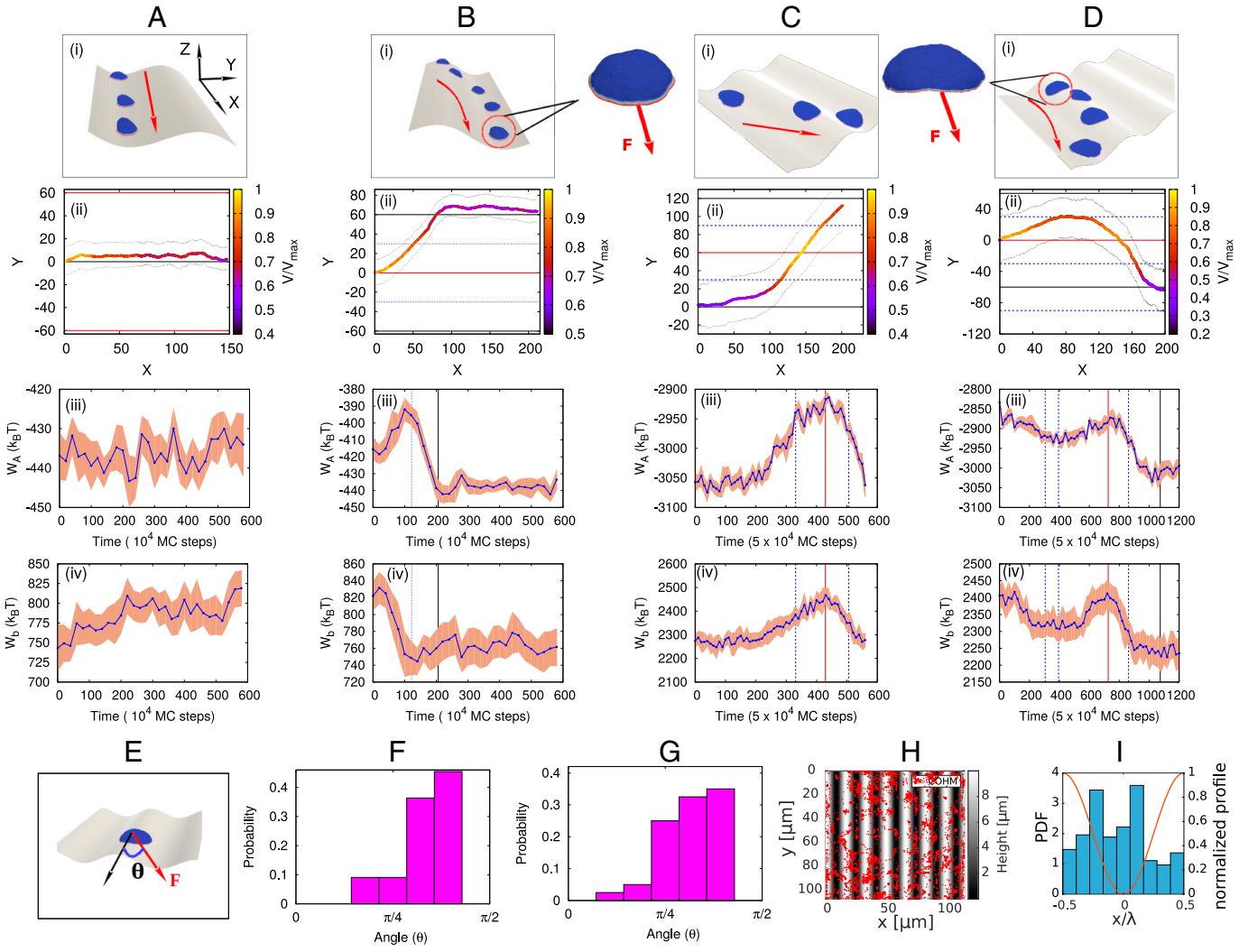

Fig. 2. Motile vesicle moving on a sinusoidal substrate with $y_m/R_{vesicle} \gg 1$. We use $z_m = 10\ l_{min}$; $y_m = 120\ l_{min}$ for sinusoidal substrate. (*A*) A small vesicle starting from the minimum of the sinusoidal substrate continues to migrate along its initial direction of migration. (*B*) Small vesicle starting from the maximum of the sinusoidal substrate shifts to the minimum of the substrate. (*C*) Large vesicle starting from the minimum of a sinusoidal substrate (with $F = 2.0\ k_BT/l_{min}$), crosses the maximum and reaches the next minimum. (*D*) Large vesicle starting from the maximum of a sinusoidal substrate (with $F = 1.0\ k_BT/l_{min}$) initially tends to migrate along the positive *Y*-axis, then changes its direction of migration toward the negative *Y*-axis, and finally reaches the minimum. Panel (*i*) shows the snapshots (with red arrows showing the direction of migration), panel (*ii*) shows the trajectories, panel (*iii*) shows the adhesion energy with time and panel (*iv*) shows the bending energy with time. (*E*) We define migration angle (θ) as the angle between the direction of migration of the vesicle (toward the net active force *F*) and the axis of the sinusoidal substrate (*x*-axis). (*F*) The distribution of angle at which the vesicle crosses the maxima, generated from simulation. Here we only use the data for large vesicle, as small vesicle in this case does not cross the ridges. (*G*) The distribution of angle at which the vesicle crosses the maxima, generated from the experimental trajectories of ref. 10. We used 40 tracks of individual cells from two replicates to generate this distribution. The statistical significance test gives $P < 10^{-9}$, where *P* is the probability that the data comes from a uniform random distribution. (*H*) The accumulated positions of center-of-mass of *Dictyostelium discoideum* cells over time. (*I*) The cumulative distribution of D.d. cell's position in a full period (λ) of the pattern. For (*H*) and (*I*), we use 105 cells, from five different replicates. Statistical significance test gives a *P* value less than 10^{-11}. For the statistical significance test, we use one-sample Kolmogorov–Smirnov test implemented in the Matlab function "kstest." For small vesicle (*A* and *B*), we use $N = 607$, $E_{ad} = 3.0\ k_BT$, $F = 4.0\ k_BT/l_{min}$ and $\rho = 4.9\%$. For large vesicle (*C* and *D*), we use $N = 3127$, $E_{ad} = 2.0\ k_BT$, and $\rho = 2.4\%$.

started in the groove (Fig. 2 *C*, *i*, *ii*), it is affected by the nearby ridge, which causes a reorientation similar to that observed in Fig. 2 *B*, *i*, *ii*. Occasionally, the larger vesicles remain aligned in the groove (*SI Appendix*, Fig. S5*A*), but its leading edge aggregate often breaks up, sometimes leading to a loss of the motile phenotype. When the larger vesicle is initiated on the ridges it reorients toward the nearby groove, but due to spanning both sides of the ridge, the vesicle can change its direction during this process (Fig. 2 *D*, *i*, *ii*). More examples of these dynamics are shown in *SI Appendix*, section S6 and Fig. S5 (Movies S6 and S7).

In order to understand this behavior, we plot the adhesion (W_A, Eq. **4**) and bending energies (W_b, Eq. **1**) of the vesicle as it is moving between the ridge and groove regions (Fig. 2 *A–D iii*, *iv*). We note that both the adhesion and bending energies are roughly constant when the vesicle migrates in the groove. When the vesicle shifts from the ridge to the groove, both the adhesion and bending energies decreases, driving the preference for the vesicle to remain inside the groove. This is easy to understand, as the vesicle can adhere more snugly when "filling" the concave groove, with lower bending energy at the vesicle rim, compared to being more curved on the ridge region. On the other hand, the curved nucleators form stronger bonds between themselves (W_d, Eq. **2**), and therefore a more robust leading edge cluster, when on the ridge (*SI Appendix*, Fig. S6). However, the changes in this energy term are small compared to the changes in the bending and adhesion energy. These observations explain why energetically it is overall more favorable for the vesicle to reside in the grooves, while the more cohesive leading edge cluster gives rise to faster motility when the vesicle crosses the ridges. Note that the cell-substrate adhesion energy was previously identified as the driving mechanism for the tendency of cells to accumulate in concave grooves and pits (27).

Our theoretical results shown in Fig. 2 *A–D*, *i*, *ii* are similar to the experimental observations of T lymphocytes migrating on sinusoidal surfaces (10). In these experiments, it was found that cells mostly migrate inside, and aligned with the grooves, while occasionally crossing the ridges rapidly and at large angles. The simulations indicate that the vesicle tends to cross the ridges at large angles (Fig. 2*F*), as observed in experiments (10) (Fig. 2*G*). A similar behavior was observed in migrating *Dictyostelium discoideum* cells on a sinusoidal substrate, as shown in Fig. 2*H* (60). The positions of the center-of-mass of the cells over time show that this cell type also tends to stay within the grooves, and avoids the ridges (Fig. 2*I*). Finally, the tendency that we find for the motile vesicle to realign such that it climbs up ridges at large angles, naturally explains the observed trajectories of T-cells climbing up ramp-like structures (61).

B. Cellular Migration on Sinusoidal Surfaces: Small Wavelength. Next, we consider the case where the vesicle radius and the wavelength of the sinusoidal undulations are of the same order, so that a vesicle spans both the ridge and the nearby groove(s). Here, we use sinusoidal variations of two types: $z_m = 1$; $y_m = 15$ and $z_m = 2$; $y_m = 30$ keeping the ratio of z_m/y_m fixed.

We find that when we start with a vesicle that is parallel to the sinusoidal pattern, the vesicle either settles at an acute angle with the axis of the sinusoidal pattern (Fig. 3*A* and Movie S8), or settles to migrate in the orthogonal direction (Fig. 3*B* and Movie S9). The speed of the vesicle shows clear oscillatory behavior (Fig. 3 *A* and *B*, *iii*). When the vesicle travels from ridge to groove, it moves toward lower energies and thereby moves faster, while in the opposite case, it slows down. These speeds seem to be periodic along the orthogonal direction to the grooves and ridges of the sinusoidal pattern. In *SI Appendix*, Fig. S7 *A* and *B*) we show the average speed of the migrating vesicle at different positions of its

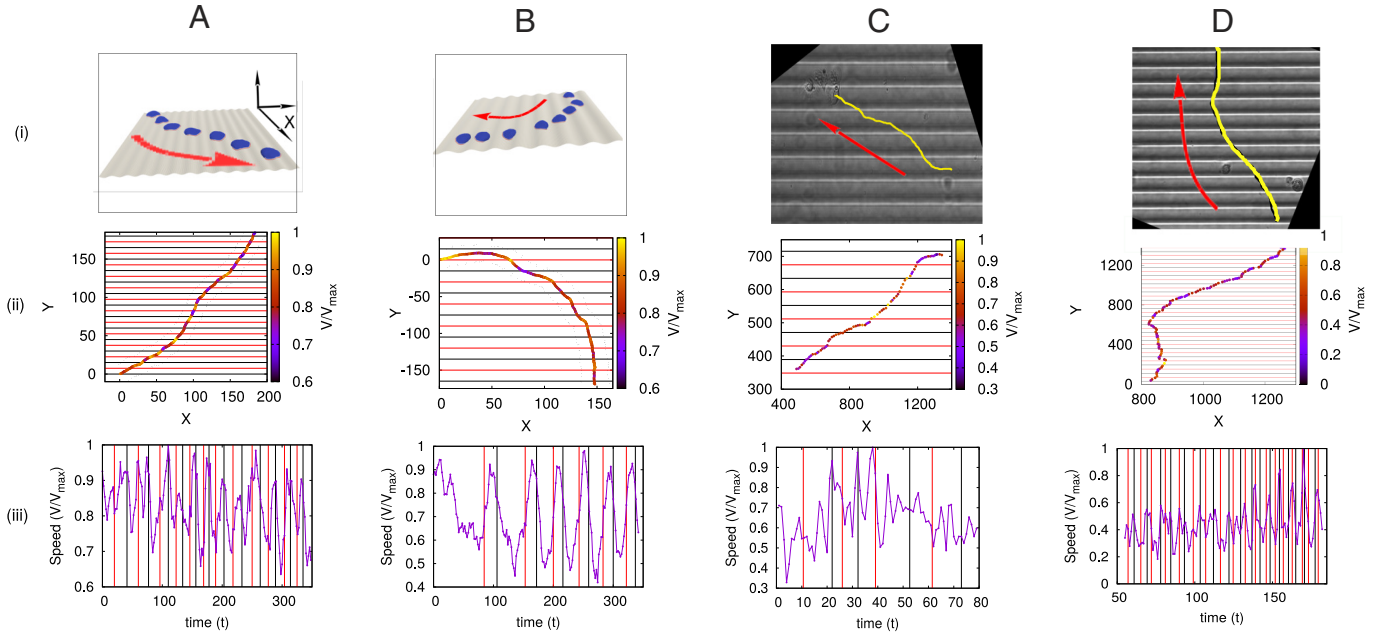

Fig. 3. Motile vesicle moving on a sinusoidal substrate with $y_m/R_{vesicle} \sim 1$. In this case, we use only a small vesicle for simulation results. (*A*) A vesicle started from the minimum of the substrate finally moves at a constant angle with the sinusoidal axis. Here, we use $z_m = 1\ l_{min}$; $y_m = 15\ l_{min}$ for the sinusoidal substrate. (*B*) A vesicle started from the maximum of the sinusoidal substrate slowly changes its migration direction and becomes orthogonal to the sinusoidal axis. Here, we use $z_m = 2\ l_{min}$; $y_m = 30\ l_{min}$ for the sinusoidal substrate. (*C*) Migrating *keratocyte* on sinusoidal pattern, that initially started along the axis, finally moves at an angle with the sinusoidal axis. This trajectory is very similar to the one observed in Fig. 3*A*. (*D*) Migrating *keratocyte*, initially at an angle and finally moves almost orthogonal to the sinusoidal axis, very similar to the trajectory in Fig. 3*B*. Here, (*i*) shows the snapshots (red arrows are showing the direction of migration), (*ii*) shows the trajectories, and (*iii*) shows the variation of speed of the vesicle/cell with time. For simulation results, we use $N = 607$, $E_{ad} = 3.0\ k_BT$, $F = 4.0\ k_BT/l_{min}$ and $\rho = 4.9\%$.

center-of-mass between two maxima of the sinusoidal pattern, showing clear periodicity.

Note that when the vesicle was aligned inside the groove (initial condition in Fig. 3*A*), it shows some tendency to persist inside the groove. This tendency gives rise to staircase-like trajectories when the vesicle moves at some oblique angle with respect to the sinusoidal pattern (Fig. 3 *A*, *ii*). We show more simulations of this type in *SI Appendix*, Fig. S8 (Movies S10 and S11).

We compare these simulations to experiments using fish keratocytes migrating on sinusoidal substrates (7), with a similar ratio of cell size and sinusoidal wavelength (Movies S12 and S13). Fish keratocytes is a perfect cellular system to be compared to vesicles since they are persistent and polarized cells that contain a large lamellipodium driven by protrusive forces exerted by actin polymerization. In Fig. 3 *C* and *D*, we show two typical trajectories, where the cell migrates in a staircase-like trajectory (Fig. 3 *C*, *i*, *ii*) or leaves the groove and moves orthogonal to the pattern (Fig. 3 *D*, *i*, *ii*); *SI Appendix*, Fig. S9 *C* and *D*). The speed of the cell shows similar oscillatory behavior as observed in our simulation (Fig. 3 *C* and *D*, *iii*). However, due to the noisy cell speed extracted from the experimental trajectories, we could not identify a clear relation between the mean speed and the cell position within the sinusoidal pattern (*SI Appendix*, Fig. S7 *C* and *D*). The experimental speed can be affected by stick-slip cellular retractions and inhomogeneities in the cell-substrate adhesion, which are absent in the simulations. In *SI Appendix*, Fig. S9 we show more experimental trajectories of migrating keratocytes on the sinusoidal substrate, similar to Fig. 3 *C* and *D* (Movies S14–S17).

The main qualitative finding is that both the cells in the experiments and the simulated vesicles have a strong tendency to move perpendicular to the wavy pattern when the cell size is comparable or larger than the wavelength of the substrate (Fig. 3). This is in stark contrast to the behavior of the cells and the simulated vesicles on a sinusoidal substrate when the cell is smaller than the wavelength of the sinusoidal pattern (Fig. 2).

In *SI Appendix*, sections S11 and S12 (Movies S18–S22), we show experimental and simulation data for cells and vesicles moving on sinusoidal surfaces of different adhesion strength. These results demonstrate the robustness of the tendency of cells to migrate persistently in the orthogonal direction to the sinusoidal pattern, thereby showing that this phenomenon does not depend on fine tuning of the system's parameters. Overall, the experimental data shown in *SI Appendix*, Fig. S11, along with the data presented in *SI Appendix*, Fig. S9, and Fig. 3 *C* and *D* shows that more than 40% cells prefer to migrate at a large angle ($60° \leq \theta \leq 90°$) with the axis of the sinusoidal pattern, which demonstrates the statistical significance of this mode of migration in comparison to the examples shown in Fig. 2, where cells prefer to migrate along the grooves of the sinusoidal pattern.

Despite the favorable comparisons between the model and the experiments on sinusoidal surfaces, it is not easy to interpret the details of the migration process on these surfaces since they contain curvatures of opposite signs. We next explore the migration pattern of our model vesicle, and living cells, on simpler curved surfaces of uniform curvature.

C. Migration Outside a Cylindrical Surface (Fiber). In order to gain a deeper understanding of the curvature-dependent motility in our model, we simulate the vesicle motion on a surface of uniform curvature, such as the convex curvature of the external surface of a cylinder (fiber). In Fig. 4*A* we plot the dynamics of a motile vesicle, when initially it was aligned along the axis of the fiber (of radius $R = 10\ l_{\min}$). We find that the vesicle spontaneously shifts its orientation, and ends up rotating along the circumferential direction, as the final steady-state of the system (Fig. 4*A* and Movie S23). This tendency, to polarize and migrate perpendicular to the axis of the fiber, explains naturally the tendency of the vesicle to migrate perpendicular to the undulation pattern, when moving over the ridges of the sinusoidal surfaces (Figs. 2 and 3).

We can understand the driving force for this re-orientation of the migration, by plotting the adhesion, bending, and protein-binding energies of the vesicle during this process (Fig. 4 *B*–*D*) as a function of the migration angle, which is defined as the angle between the direction of motion and the fiber axis (see *SI Appendix*, sections S13 and S14 and Figs. S12 and S13 for more details). We see that there is a small gain in adhesion (decrease in adhesion energy), decrease in overall bending energy, and a small decrease in the protein binding energy. When oriented circumferentially, the leading edge active forces can stretch the vesicle sideways along the cylinder's axis, which is efficient in increasing the adhered area along a direction of low curvature, by keeping the membrane close to the fiber surface (Fig. 4*E*). By comparison, when the vesicle is oriented along the axis (Fig. 4*F*) only a small region of the leading edge, along the axis, can pull the membrane close to the fiber and maintain its adhesion. The parts of the leading edge that point along the circumferential direction are less effective in increasing the adhered area due to pulling the membrane off the surface, as well as increasing its bending energy.

This predicted tendency for cells to rotate around fibers, when their migration is driven by a lamellipodial protrusion, is nicely verified by experimental data on *Dictyostelium discoideum* cells (12). The observed trajectories of migration are biased along the circumferential direction (Fig. 4*G* and Movie S24), as shown by the peak in the distribution of cellular migration direction (Fig. 4*I*). The speed of the cells was also found to be maximal along the circumferential direction (Fig. 4*H*).

Furthermore, it was found experimentally that the tendency of the cells to migrate circumferentially decreased as the fiber radius increased (*SI Appendix*, Fig. S14) (12). Our model can offer an explanation of this trend, as we find that the energetic advantage of the circumferential orientation in our simulations decreases with increasing fiber radius.

A similar tendency was observed for motile MDCK cells on a fiber (Movie S25). The trajectories in Fig. 4*J* show that these cells were either migrating in highly persistent bursts along the circumferential direction, or moving in a more random motion along the axial direction (while the speed exhibits no clear angular dependence, see *SI Appendix*, Fig. S15). This agrees with the model's prediction that the lamellipodia's leading edge is more robust along the circumferential direction, which should result in more persistent motion along this direction.

Previous studies with MDCK cells moving on very thin fibers (fiber cross-section circumference same or smaller than the cell diameter) reported a bi-phasic migration pattern (20). Isolated cells were sometimes observed to migrate axially with high speed, and with a very small adhered surface area. The cell body in these cases exhibits a highly rounded shape, typical of cells under strong contractile forces. Such contractile forces are outside the present model, and we therefore do not expect to reproduce this axially motile phenotype (62). However, a second phenotype was observed in these experiments, when cells spread and adhere

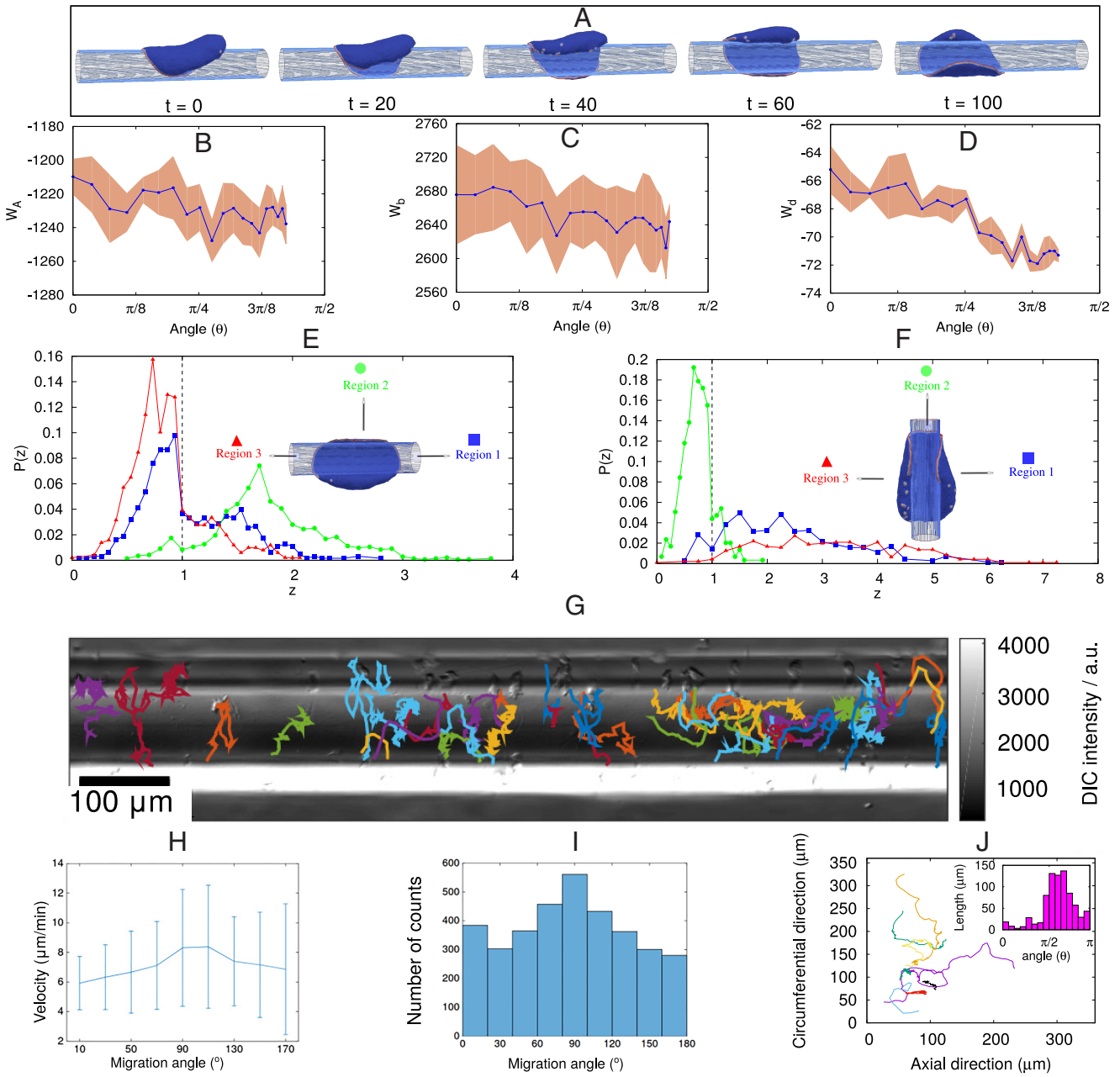

Fig. 4. Vesicle migrating outside of a cylindrical fiber. (*A*) Configurations of the motile vesicle migrating on a fiber, initially in the axial direction, and finally reorients to rotate circumferentially. (*B*) The adhesion, (*C*) bending, and (*D*) binding energies of the vesicle as function of its migration angle during the reorientation process shown in (*A*). (*E*) Distribution of the distance z of a curved protein along the leading edge from the cylindrical surface, when the vesicle is oriented circumferentially. We plot this distance distribution for three different sections of the leading edge, along three directions, as defined in the *Inset*. The part of the distributions that are on the *Left* side of the vertical dashed line (at $z = 1$) represent adhered proteins. (*F*) Same as (*E*), when the vesicle is oriented axially. (*G*) Trajectories of different D.d. cells on the fiber of diameter 160 μm (12). (*H*) The distribution of migration speeds of D.d. cells, as function of the migration angle, where 0 or π represent the axial direction and $\pi/2$ represents the circumferential direction. (*I*) Distribution of migration angles of D.d. cells on the fiber, as in (*H*). In (*G–I*), we use 42 trajectories of different cells. The *P*-value that the data come from a uniform random distribution is less than 10^{-11}. (*J*) The trajectories of MDCK cells migrating on a fiber of 50 to 70 μm in diameter. *Inset* shows the distribution of total path length covered by the cell in 10 min durations as function of the angular direction, as in (*I*). Here, we use trajectories of nine cells in three independent experiments. The statistical significance test for path length distribution gives $P < 10^{-12}$. We use Matlab function "kstest" for the statistical significance test. For simulation results, we use the radius of the fiber $R = 10\, l_{\min}$, $F = 2.0\, k_BT/l_{min}$, $E_{ad} = 1.0\, k_BT$ and $\rho = 2.4\%$.

strongly to the fiber surface. During these times the cells seem to exhibit short rotation periods around the fiber circumference (20), but their durations were too short to be conclusive. In addition, the overall orientation of the actin fibers in a confluent monolayer of cells on the fiber was found to be circumferential, in agreement with the orientation of the isolated cell in our simulations.

Another example for spontaneous rotational migration of cells on cylindrical surfaces is shown in Fig. 5 *A–C* (Movies S26 and S27). Here *Dictyostelium discoideum* cells are shown to rotate persistently on the external surface of pillars with circular cross-section. On pillars with triangular cross-section, we find that the cells slow down periodically whenever they cross the higher curvature corners (Fig. 5 *D* and *E*). In *SI Appendix*, Fig. S17

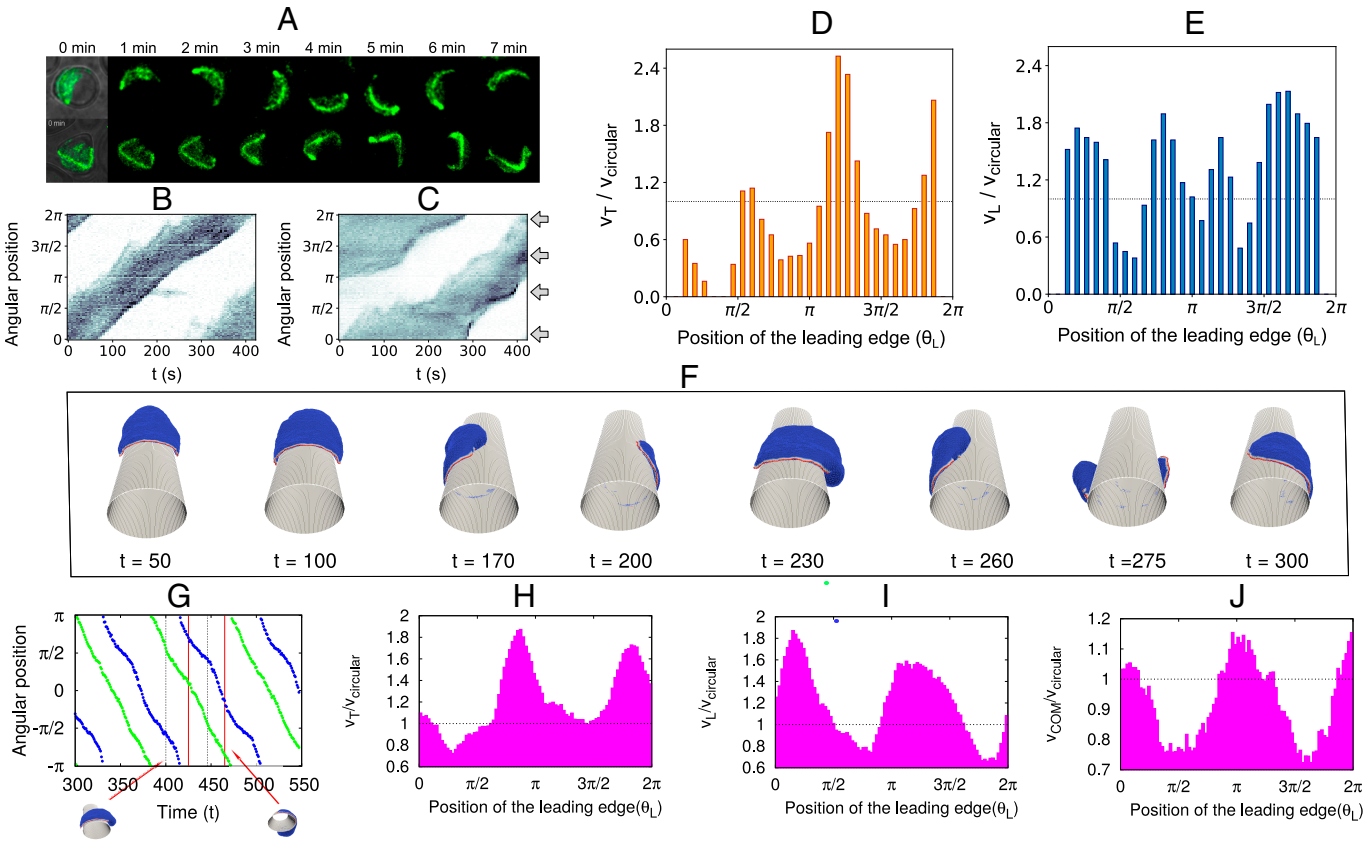

Fig. 5. Curvature sensing on micropillars. (*A*) Timelapse snapshots of *Dictyostelium discoideum* cells moving along the surface of a circular (*Top*) or triangular (*Bottom*) shaped micropillar. In both cases, the field of view shown is 30 × 30 um. Cells express LifeAct-GFP. (*B*) Kymograph of the actin signal for the cell shown in (*A*) on the round micropillar. The intensity has been integrated in each angular slice and color coded from white (0) to black (max). (*C*) Same as (*B*) for the triangular-shaped pillar. The arrows indicate the positions where the triangle corners are located. (*D*) Variation in the speed of the trailing edge V_T (scaled by the average speed for the fiber with circular cross-section) as a function of the position of the leading edge (θ_L). (*E*) Variation in the speed of the leading edge (V_L) as a function of the position of the leading edge (θ_L). (*F*) Snapshots of the migrating vesicle on a fiber with elliptical cross-section with aspect ratio $r = 1.54$. The vesicle initially migrates in the axial direction and finally reorients along the circumferential direction for longer time ($t > 200$). (*G*) Kymograph of the leading edge (blue circles) and the trailing edge (green circles) when the vesicle is rotating circumferentially ($t > 300$). (*H*) Speed of the trailing edge of the vesicle V_T (scaled by the speed for the fiber with circular cross-section $V_{circular}$) as a function of the position of the leading edge (θ_L) over a full period. (*I*) Speed of the leading edge of the vesicle V_L as a function of the position of the leading edge (θ_L) over a full period. (*J*) Speed of the center of mass (com) of the vesicle V_{COM} as a function of the position of the leading edge (θ_L) over a full period. For simulation, we use $R_x = 12\, l_{\min}$, $R_y = 7.773\, l_{\min}$, $E_{ad} = 1.5\, k_BT$, $F = 2.0\, k_BT/l_{\min}$, and $\rho = 2.4$ %.

we present several additional experimental kymographs for cells performing persistent rotations around micropillars of circular cross-section.

Note that when cells are migrating on extremely thin fibers, the motility mode is very different, driven by elongated and thin protrusions on either side of the cell (62). There is no single lamellipodium that drives the migration, and no global rotation of the cell around the fiber. However, the leading edges of the protrusions tend to coil around the fiber. We suggest that this behavior is driven by the same mechanism that we identified here to cause global rotations on larger fibers (47).

In order to verify the above predictions, we simulated the migration of the motile vesicle on a fiber of elliptical cross-section, such that the rotating vesicle experiences different curvatures periodically (Fig. 5*F* and Movie S28). By plotting the kymograph (Fig. 5*G*) and the speed as function of position (Fig. 5 *H*–*J*), we find periodic variations in the speed of the vesicle that are similar to those observed in the experiments (Fig. 5 *B*–*E*). Note that the experiments exhibit three peaks, due to the triangular shape, compared to two peaks in the simulations on the elliptic cross-section.

In *SI Appendix*, section S19 and Fig. S18, we compare the dynamics of migrating vesicles on elliptical fibers of different aspect ratio $r = R_x/R_y$. We note that it takes more time for the vesicle to reorient toward the circumferential direction as the aspect ratio r increases (*SI Appendix*, Fig. S18 *A* and *B*). For the largest aspect ratio that we tested ($r = 2.87$), the vesicle does not reorient at all (*SI Appendix*, Fig. S18*C*), due to the sharp corners that present bending energy barriers. This inhibition of rotation over the sharp corners is similar to the inhibition of coiling at the leading edge of cellular protrusions, calculated and observed when cells spread over fibers (47).

At higher adhesion strength, the simulated vesicle rotates faster from axial to circumferential orientation (see *SI Appendix*, section S20 and Fig. S19 and Movie S29 for details). This trend is qualitatively observed in MDCK cells which exhibit a reduced preference to migrate along the circumferential direction compared with a fiber of higher adhesion strength, as predicted in simulation (compare *SI Appendix*, section S21 and Fig. S20 with Fig. 4*J*). However, more research using several cell types is needed in order to further verify these predictions in experiments.

D. Migration Inside a Cylindrical Surface (Tube). Next, we study the migration of cells inside a cylindrical tube, a uniformly concave surface. We start with our vesicle, that shows no tendency to rotate circumferentially when initially aligned to migrate along the axial direction (Fig. 6*A* and Movie S30). Over time, the vesicle is found to lose its motility, and the leading edge protein cluster breaks into several parts, which leads to a decrease in the total active force that propels the vesicle (Fig. 6*B*). This is similar to the behavior inside the grooves of the sinusoidal surface (Fig. 2 *A* and *B*). We chose here a tube radius such that the circumference of the tube is much larger than the vesicle's diameter. In this regime we can explore the cell migration on the surface, avoiding "plugging" of the tube by the vesicle when the tube radius is smaller than the cell radius (21).

The different energy terms of the vesicle do not show any systematic variation during its migration in the tube (Fig. 6 *C*–*E*). In Fig. 6*F* we show that all the proteins along the cell edge are well adhered to the substrate, which is why the leading edge can easily break up and form clusters along any direction. The leading-edge that was initially oriented axially, will tend to break into two arcs that point side-ways. This destabilizes the polarized leading-edge aggregate, and the cell migration slows down, sometimes to a halt (forming a two-arc non-motile phenotype). As a result, we find that the vesicle in the tube ends up either as slowly migrating in the axial direction (on average, Fig. 6*A*) or a two-arc (nonmotile) vesicle that can be axial or "bridge" orthogonally to the axis (*SI Appendix*, Fig. S21 and Movie S31).

Comparing to experimental observations of cells moving inside tubes (63), it was indeed found that cells tend to migrate along the tube axis, as we obtain (Fig. 6*A*). However, this tendency is strongly cell-type dependent, with some cells becoming nonmotile inside tubes, forming adhesion "bridges" that can be orthogonal to the tube axis (16). This observation agrees with our finding that the motility inside the tube is strongly inhibited, with the cells tending to lose their polarization (Fig. 6 *A* and *B*). In ref. 21, it was indeed observed that the motility along the

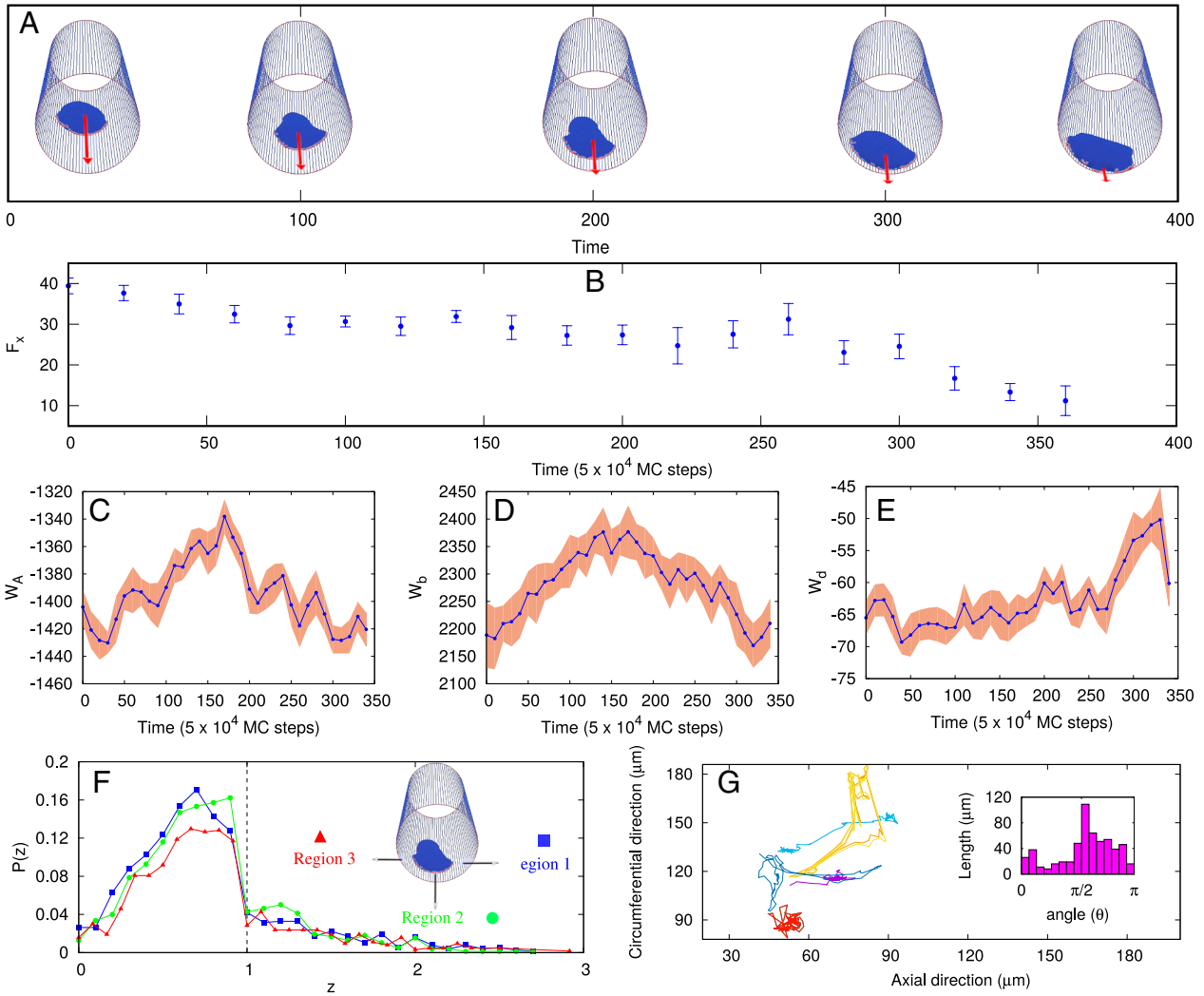

Fig. 6. Vesicle migrating inside a cylindrical tube. (*A*) Configuration of vesicle migrating inside a tube, initiated in the axial direction. (*B*) Magnitude of active force along the axis of cylinder (F_X) with time. (*C*) The adhesion energy of the vesicle with time. (*D*) The bending energy of the vesicle with time. (*E*) The binding energy between proteins with time. (*F*) Probability distribution of a protein at z distance above the cylindrical substrate. The left side of the vertical dashed line (at $z = 1$) represents adhered proteins. Here, we use $R = 35\ l_{min}$, $E_{ad} = 1.0\ k_BT$, $F = 2.0\ k_BT/l_{min}$, and $\rho = 2.4\%$. (*G*) Trajectories of the MDCK cells migrating inside tubes of 67 to 75 μm in diameter. *Inset* shows the distribution of total path length covered by the cell in 10 min durations as function of direction, where 0,π represent the axial direction, and $\pi/2$ represents the circumferential direction. We used trajectories of seven cells in three independent experiments. Statistical significance test for path length data gives $P < 10^{-12}$. We use Matlab function "kstest" for the statistical significance test. This indicates that while the angular distribution is not uniform, it is more evenly spread compared to the case of migration on the fiber (*inset* of Fig. 4*J*).

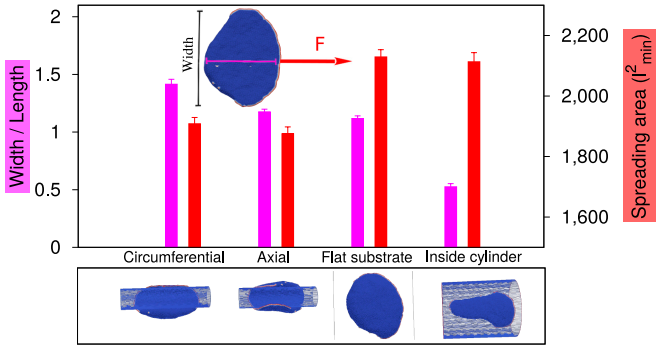

Fig. 7. Ratio of the length (along *F*) and width (orthogonal to *F*) of the vesicle and the spreading area, for four different cases when it is moving (1) along circumferential direction on a cylinder, (2) along axial direction on a cylinder, (3) on a flat substrate and (4) inside of a cylindrical tube. The magenta color is for the aspect ratio and the red color showing the spreading area. *Inset* shows a crescent shape on a flat substrate, defining the length and the width of the vesicle. For fiber, we use $R = 10\ l_{min}$, for tube, we use $R = 35\ l_{min}$. Other parameters are $F = 2.0$, $E_{ad} = 1.0$ and $\rho = 2.4\%$.

tube axis decreases as the tube radius decreases, as cells migrate less persistently, and their leading-edge lamellipodia becomes less persistent and less stable. In addition, the overall orientation of actin filaments for cells inside tubes was axial, in qualitative agreement with our model's results. Our theoretical predictions are also in agreement with recent observations of keratocytes moving inside cylindrical grooves (63), which were observed to move more slowly compared to flat surface and undergo large shape changes.

Fig. 6*G*, we show the trajectories for the migration of MDCK cells on the inside of a tube. The cells were found to be weakly motile, with trajectories exhibiting no clear directional dependence (Movie S32), in agreement with the model predictions. We also presented a directional consistency test for MDCK cells on fiber as well as inside the tube and show the details in *SI Appendix*, section S17 and Fig. S16. Individual cells are found to migrate consistently for more than 8 h on fibers but usually less than 1 h inside tubes. Statistical significance test for this analysis gives P value < 0.05.

Another recent study (64) on two cell types (endothelial and epithelial cells), found similar axial alignment of the cells' shape and their migration inside tubes. However, the role of stress fibers, which we do not include in our model, was suggested to have a major role for these cells.

In Fig. 7 we summarize the steady-state shapes for the simulated motile vesicles on the different curved substrates (except for the "axial" configuration on the fiber, which is not at steady-state). We note that the adhered area is maximal for a flat substrate, but is not very different when the vesicle is inside the tube, where it is also well adhered. When on the fiber, moving in the axial direction, the adhered area is the smallest, and it is slightly larger when moving in the circumferential direction. The aspect ratio shows that the active force is able to stretch the vesicle sideways along the axis of the tube, when it is oriented circumferentially. The highly elongated shape of the aligned cell moving in the tube, compared to the flat substrate, fits well with the observed elongation of the cells when migrating inside the grooves of the sinusoidal substrate (10).

3. Conclusion

We demonstrated here that a minimal physical model of a motile cell, based on very few ingredients and energy terms, is able to describe and explain several qualitative features of curvotaxis of lamellipodia-based cell migration on curved adhesive substrates. Within this minimal model, cell migration arises when a leading edge cluster of highly curved membrane protein complexes forms, due to these protein complexes being both highly curved, binding to each other and exerting protrusive forces on the membrane. These forces represent in the model the pressure exerted on the membrane when actin polymerization is initiated at the membrane by these curved protein complexes, which contain actin nucleation factors such as WAVE (51–53). The curvotaxis features that the model explains, such as the tendency of motile cells to migrate aligned within grooves, avoid ridges, and rotate around fibers, all arise due to minimization of the adhesion and bending energies of the vesicle. The advantage of simple, physical models is demonstrated here, exposing general mechanisms that are universal and not cell-type-specific. The model makes qualitative predictions that potentially apply to many cell types. For example, our model predicts that when the cell size is small compared to the sinusoidal pattern wavelength the migration will tend to remain along the pattern, as found for T-lymphocytes (10) and shown here for *Dictyostelium discoideum*. At the same time, the model predicts that the migration becomes orthogonal to the sinusoidal pattern when the cell size is comparable or larger than the pattern's wavelength, as verified here for keratocytes.

The curvotaxis property of the motile "minimal-cell" is shown to be a truly emergent phenomenon of the whole motile vesicle. Within our model, the energy minimization that aligns the migration of the "minimal-cell" arises from shape changes of the whole vesicle in response to the imposed curved surface and the organization of the curved membrane complexes that form the leading-edge cluster (and motility). The curved membrane complexes are sensitive to curvature on a much smaller length-scale compared to the cell size and therefore do not directly determine the preferred curvotaxis response of the whole motile vesicle.

Eukaryotic cells contain numerous additional components that our simple model does not contain, such as the effects of contractility, stress fibers, and internal organelles (such as the large nucleus), which can all affect migration on curved substrates. Nevertheless, the agreement between the predictions of the model and the observations of curvotaxis in different types of motile cells, suggests that these simple energetic considerations may drive curvotactic features in cells, despite the biochemical complexity and differences between cells. These results demonstrate that complex cellular behavior may have physical underpinnings, with added layers of biological complexity and regulation. The framework presented here could serve in the future to explore cell migration in more complex geometries (11, 65), and over soft substrates (such as other cells) with dynamic curvature.

4. Materials and Methods

Here, we describe our experimental methods briefly. More details are given in *SI Appendix*, section S2.

A. Migrating Keratocytes on Sinusoidal Substrate. Fish epithelial keratocytes were obtained from the scales of Central American cichlid (Hypsophrys Nicaraguensis) (7, 66). Scales were gently taken off the fish and placed overnight at room temperature between two clean glass coverslips with a drop of 150 μL of culture medium. Corrugated polyacrylamide hydrogels were fabricated by photopolymerization with an Irgacure 2959 photoinitiator (2-Hydroxy-4′-(2-hydroxyethoxy)-2-methylpropiophenone) to polymerize hydroxypolyacrylamide (hydroxy-PAAm) hydrogels (23). Hydroxy-polyacrylamide (hydroxy-PAAm) hydrogels were prepared by mixing acrylamide (AAm), bis-acrylamide

(bis-AAm), N-hydroxyethylacrylamide (HEA), 2-Hydroxy-4′-(2-hydroxyethoxy)-2-methylpropiophenone (Irgacure 2959, Sigma #410896) and deionized water (67). Time-lapse microscopy experiments were carried out on a Nikon Ti-U inverted microscope (Nikon, Japan) equipped with Differential Interference Contrast (DIC) mode. More details are given in *SI Appendix*, section S2A.

B. Migration of *Dictyostelium discoideum* (D. d.) Cells on Sinusoidal and Cylindrical Substrates. In order to prepare cell axenic D.d. lines for experiments, frozen stock was thawed at room temperature and afterward cultured in HL5 medium on Petri dishes. The doubling time of the cells was between 8 and 9 h at the optimal growing temperature of 21 to 23 °C. The cell culture was subcultured every 2 to 3 d, when the cells have become confluent in the Petri dish. For the experiments on glass capillaries, we placed the optical fibers in a perfusion chamber (RC-27, Large Bath Chamber, Warner Instruments, Hamden, CT, USA) on a glass-spacers to allow a fluid flow around the fiber or used a microfluidic device with through flow. For the experiments on sinusoidal substrate, we use the Photonic Professional (GT) (Nanoscribe) to produce masks for sinusoidal substrates. We chose IP-S, a highly viscous photoresist, in combination with a 25× objective (ZEISS 25×/0,8 DIC Imm Korr LCI Plan-NEOFLUAR) and an ITO-coated DiLL glass substrate (size 25mm × 25 mm; thickness 0.7 mm; optical transparent; provided by NanoScribe) for the mask production. See *SI Appendix*, section S2B for more details.

C. Spreading and Migration of *Madin-Darby Canine kidney* (MDCK) Cells on Fibers and Inside Tube. MDCK-LifeAct-GFP (stable cell line transfected with LifeAct GFP, binding to actin filaments) cells were cultured in complete DMEM (Life Technologies), supplemented with 10% fetal bovine serum and 1% penicillin/streptomycin). Cells were cultured at 37°C and 5% CO_2 conditions until confluent. Microtubes were fabricated inside polydimethylsiloxane (PDMS) blocks using previously described method (21). To record a 3D, live-cell video, z-stacks (1 μm per Z step) covering the whole volume of PDMS microfibers or microtubes were recorded at 10 min/frame with either 25×, 40× or 63× objectives. 3D time-lapse videos were recorded over a period ranging from 10 to 24 h. For more details, see *SI Appendix*, section S2C.

D. Migration of *Dictyostelium discoideum* (D. d.) Cells on Micropillars. The non-axenic *D. discoideum* strain DdB NF1 KO (68), transformed with an episomal plasmid encoding for Lifeact-GFP and PHcrac-RFP (SF108, as described in ref. 69) was used. Cells were cultivated in 10 *cm* dishes with Sørensen's buffer (14.7 mM KH_2PO_4, 2mM Na_2HPO_4, pH 6.0) supplemented with 50 μM $MgCl_2$, 50 μM $CaCl_2$ and using G418 (5 μg/ml) and hygromycin (33μg/ml) as selection markers. For the microfabrication of pillar structures, a silicon wafer was coated with a 10 μm photoresist layer (SU-8 2010, Micro Resist Technology GmbH, Germany) and patterned by direct-write lithography using a maskless aligner (μMLA, Heidelberg Instruments Mikrotechnik GmbH, Germany). The cells were diluted to a density that enabled imaging of single cells on the surface of the pillars. Temporal recordings were acquired at a rate of 0.2 fps using a laser scanning microscope (LSM780, Zeiss, Jena) with a 488-nm Argon laser and a 40× water immersion objective. For more details, see *SI Appendix*, section S2D.

Data, Materials, and Software Availability. All code for conducting simulations with configuration files for acquisition of the results associated with the current submission is openly available at GitHub https://github.com/rajsadhu3903/curvotaxis-codes. Any future updates will also be published in the same GitHub repository (70). All study data are included in the article and/or supporting information.

ACKNOWLEDGMENTS. We thank Junsang Doh and collaborators for providing the data for the migration of T lymphocytes on sinusoidal wavy surfaces. N.S.G. is the incumbent of the Lee and William Abramowitz Professorial Chair of Biophysics, and acknowledges support by the Ben May Center for Theory and Computation, and the Israel Science Foundation (Grant No. 207/22). This research is made possible in part by the historic generosity of the Harold Perlman Family. R.K.S. acknowledges the support from ANR (ANR-19-CE11-0002-03). A.I. and S.P. were supported by the Slovenian Research Agency (ARIS) through the Grants No. J3-3066 and J2-4447 and Programme No. P2-0232. This work was supported by the Marie Skłodowska-Curie Actions, Individual Fellowship, Project: 846449 (to W.X.) and the Labex Who Am I? (ANR-11-LABX-0071) and the "Initiatives d'excellence" (Idex ANR-11-IDEX-0005-02) transverse project BioMechanOE (TP5) (to W.X.). This work was supported by the European Research Council (Grant No. Adv-101019835 to B.L.), LABEX Who Am I? (ANR-11-LABX-0071 to B.L.) and the Ligue Contre le Cancer (Equipe labellisée 2019 to B.L. and W.X.) and the ANR PRC LUCELL grant (ANR-19-CE13-0014-01 to B.L. and W.X.), and DIM-ELICIT 2019: Equipment support, Région Ile-de-France (to W.X. and B.L.). B.L. and W.X. acknowledge the ImagoSeine core facility of the IJM, member of IBiSA and France-BioImaging (ANR-10-INBS-04) infrastructures. W.X. acknowledges Yuan Shen for the calculation of the correlation time of velocity. The research of Carsten Beta and C.M.-T. has been partially funded by the Deutsche Forschungsgemeinschaft (DFG), Project-ID No. 318763901–SFB1294. S.G. acknowledges funding from FEDER Prostem Research Project no. 1510614 (Wallonia DG06), the F.R.S.-FNRS Epiforce Project no. T.0092.21, the F.R.S.-FNRS Cellsqueezer Project no. J.0061.23, the F.R.S.-FNRS Optopattern Project no. U.NO26.22 and the Interreg MAT(T)ISSE project, which is financially supported by Interreg France-Wallonie-Vlaanderen (Fonds Européen de Développement Régional, FEDER-ERDF). S.G. thanks Programme Wallon d'Investissement R'egion Wallone pour les instruments d'imagerie (INSTIMAG UMONS #1910169). M.L. is Chargée de Recherches F.R.S-FNRS and financially supported by the WBI-World Excellence Grant Programme for long-term scholarship. M.L. and S.G. acknowledge Alexandre Remson and Marie Versaevel for technical support.

Author affiliations: [a]Department of Chemical and Biological Physics, Weizmann Institute of Science, Rehovot 7610001, Israel; [b]Department of Biochemistry, University of Geneva, Geneva 4 CH-1211, Switzerland; [c]Mechanobiology & Biomaterials Group, Research Institute for Biosciences, Center of Innovation and Research in Materials and Polymers, University of Mons, Mons B-7000, Belgium; [d]Universite Paris Cite, CNRS, Institut Jacques Monod, Paris F-75013, France; [e]Institute of Physics and Astronomy, University of Potsdam, Potsdam 14476, Germany; [f]Department of Fluid Physics, Pattern Formation and Biocomplexity, Max Planck Institute for Dynamics and Self-Organization, Göttingen 37077, Germany; [g]Laboratory of Physics, Faculty of Electrical Engineering, University of Ljubljana, Ljubljana 1000, Slovenia; [h]Nano Life Science Institute, Kanazawa University, Kanazawa 920-1192, Japan; and [i]Department of Chemistry and Biochemistry, Florida State University, Tallahassee, FL 32306-4390

Author contributions: R.K.S., S.P., A.I., C.B., O.S., E.B., B.L., S.G., and N.S.G. designed research; R.K.S., M.L., W.X., C.M.-T., M.S., C.B., M.T., S.V., and S.G. performed research; R.K.S., M.L., W.X., C.M.-T., M.S., C.B., M.T., S.V., C.B., and O.S. analyzed data; and R.K.S., A.I., E.B., B.L., S.G., and N.S.G. wrote the paper.

1. J. Howard, *Mechanics of Motor Proteins and the Cytoskeleton* (Sinauer Associates, Sunderland, MA, United States, 2001).
2. P. Friedl, D. Gilmour, Collective cell migration in morphogenesis, regeneration and cancer. *Nat. Rev. Mol. Cell Biol.* **10**, 445–457 (2009).
3. H. G. Döbereiner, B. Dubin-Thaler, G. Giannone, H. S. Xenias, M. P. Sheetz, Dynamic phase transitions in cell spreading. *Phys. Rev. Lett.* **93**, 108105 (2004).
4. E. A. Cavalcanti-Adam *et al.*, Cell spreading and focal adhesion dynamics are regulated by spacing of integrin ligands. *Biophys. J.* **92**, 2964–2974 (2007).
5. D. Cuvelier *et al.*, The universal dynamics of cell spreading. *Curr. Biol.* **17**, 694–699 (2007).
6. M. Théry *et al.*, Anisotropy of cell adhesive microenvironment governs cell internal organization and orientation of polarity. *Proc. Natl. Acad. Sci. U.S.A.* **103**, 19771–19776 (2006).
7. D. Mohammed *et al.*, Substrate area confinement is a key determinant of cell velocity in collective migration. *Nat. Phys.* **15**, 858–866 (2019).
8. T. Chen *et al.*, Large-scale curvature sensing by directional actin flow drives cellular migration mode switching. *Nat. Phys.* **15**, 393–402 (2019).
9. G. Dunn, J. Heath, A new hypothesis of contact guidance in tissue cells. *Exp. Cell Res.* **101**, 1–14 (1976).
10. K. H. Song, S. J. Park, D. S. Kim, J. Doh, Sinusoidal wavy surfaces for curvature-guided migration of T lymphocytes. *Biomaterials* **51**, 151–160 (2015).
11. L. Pieuchot *et al.*, Curvotaxis directs cell migration through cell-scale curvature landscapes. *Nat. Commun.* **9**, 1–13 (2018).
12. C. Blum, Ph.D. thesis (Georg August University of Göttingen, 2015).
13. S. J. Callens, R. J. Uyttendaele, L. E. Fratila-Apachitei, A. A. Zadpoor, Substrate curvature as a cue to guide spatiotemporal cell and tissue organization. *Biomaterials* **232**, 119739 (2020).
14. R. K. Assoian, N. D. Bade, C. V. Cameron, K. J. Stebe, Cellular sensing of micron-scale curvature: A frontier in understanding the microenvironment. *Open Biol.* **9**, 190155 (2019).
15. M. Werner, N. A. Kurniawan, G. Korus, C. V. C. Bouten, A. Petersen, Mesoscale substrate curvature overrules nanoscale contact guidance to direct bone marrow stromal cell migration. *J. R. Soc. Interface* **15**, 20180162 (2018).

16. M. Werner, A. Petersen, N. A. Kurniawan, C. V. C. Bouten, Cell-perceived substrate curvature dynamically coordinates the direction, speed, and persistence of stromal cell migration. *Adv. Biosyst.* **3**, 1900080 (2019).
17. Y. Y. Biton, S. A. Safran, The cellular response to curvature-induced stress. *Phys. Biol.* **6**, 046010 (2009).
18. J. A. Sanz-Herrera, P. Moreo, J. M. García-Aznar, M. Doblaré, On the effect of substrate curvature on cell mechanics. *Biomaterials* **30**, 6674–6686 (2009).
19. M. Werner, N. A. Kurniawan, C. V. Bouten, Cellular geometry sensing at different length scales and its implications for scaffold design. *Materials* **13**, 963 (2020).
20. H. G. Yevick, G. Duclos, I. Bonnet, P. Silberzan, Architecture and migration of an epithelium on a cylindrical wire. *Proc. Natl. Acad. Sci. U.S.A.* **112**, 5944–5949 (2015).
21. W. Xi, S. Sonam, T. B. Saw, B. Ladoux, C. T. Lim, Emergent patterns of collective cell migration under tubular confinement. *Nat. Commun.* **8**, 1–15 (2017).
22. M. B. Mazalan, M. A. B. Ramlan, J. H. Shin, T. Ohashi, Effect of geometric curvature on collective cell migration in tortuous microchannel devices. *Micromachines* **11**, 659 (2020).
23. M. Luciano *et al*., Cell monolayers sense curvature by exploiting active mechanics and nuclear mechanoadaptation. *Nat. Phys.* **17**, 1382–1390 (2021).
24. A. Glentis *et al*., The emergence of spontaneous coordinated epithelial rotation on cylindrical curved surfaces. *Sci. Adv.* **8**, eabn5406 (2022).
25. W. Tang *et al*., Collective curvature sensing and fluidity in three-dimensional multicellular systems. *Nat. Phys.* **18**, 1371–1378 (2022).
26. S. Z. Lin, Y. Li, J. Ji, B. Li, X. Q. Feng, Collective dynamics of coherent motile cells on curved surfaces. *Soft Matter* **16**, 2941–2952 (2020).
27. M. Vassaux, L. Pieuchot, K. Anselme, M. Bigerelle, J. L. Milan, A biophysical model for curvature-guided cell migration. *Biophys. J.* **117**, 1136–1144 (2019).
28. X. He, Y. Jiang, Substrate curvature regulates cell migration. *Phys. Biol.* **14**, 035006 (2017).
29. B. Winkler, I. S. Aranson, F. Ziebert, Confinement and substrate topography control cell migration in a 3D computational model. *Commun. Phys.* **2**, 1–11 (2019).
30. G. Honda *et al*., Microtopographical guidance of macropinocytic signaling patches. *Proc. Natl. Acad. Sci. U.S.A.* **118**, e2110281118 (2021).
31. I. Manifacier *et al*., In silico analysis shows that dynamic changes in curvature guide cell migration over long distances. *Biomech. Mod. Mechanobiol.* (2023).
32. M. Fošnarič *et al*., Theoretical study of vesicle shapes driven by coupling curved proteins and active cytoskeletal forces. *Soft Matter* **15**, 5319–5330 (2019).
33. R. K. Sadhu, S. Penič, A. Iglič, N. S. Gov, Modelling cellular spreading and emergence of motility in the presence of curved membrane proteins and active cytoskeleton forces. *Euro. Phys. J. Plus* **136**, 495 (2021).
34. N. Ramakrishnan, P. Sunil Kumar, J. H. Ipsen, Membrane-mediated aggregation of curvature-inducing nematogens and membrane tubulation. *Biophys. J.* **104**, 1018–1028 (2013).
35. C. Schmeiser, C. Winkler, The flatness of lamellipodia explained by the interaction between actin dynamics and membrane deformation. *J. Theor. Biol.* **380**, 144–155 (2015).
36. H. Alimohamadi, P. Rangamani, Modeling membrane curvature generation due to membrane-protein interactions. *Biomolecules* **8**, 1–25 (2018).
37. L. Mesarec, M. Drab, S. Penič, V. Kralj-Iglič, A. Iglič, On the role of curved membrane nanodomains, and passive and active skeleton forces in the determination of cell shape and membrane budding. *Int. J. Mol. Sci.* **22**, 2348 (2021).
38. M. Chabanon, J. C. Stachowiak, P. Rangamani, Systems biology of cellular membranes: A convergence with biophysics. *WIREs Syst. Biol. Med.* **9**, e1386 (2017).
39. J. Linkner *et al*., The inverse BAR domain protein IBARa drives membrane remodeling to control osmoregulation, phagocytosis and cytokinesis. *J. Cell Sci.* **127**, 1279–1292 (2014).
40. I. Begemann *et al*., Mechanochemical self-organization determines search pattern in migratory cells. *Nat. Phys.* **15**, 848–857 (2019).
41. A. Pipathsouk *et al*., The wave complex associates with sites of saddle membrane curvature. *J. Cell Biol.* **220**, e202003086 (2021).
42. A. B. Verkhovsky, T. M. Svitkina, G. G. Borisy, Self-polarization and directional motility of cytoplasm. *Curr. Biol.* **9**, 11–S1 (1999).
43. R. M. Lee *et al*., Quantifying topography-guided actin dynamics across scales using optical flow. *Mol. Biol. Cell* **31**, 1753–1764 (2020).
44. R. M. Brunetti *et al*., Wasp integrates substrate topology and cell polarity to guide neutrophil migration. *J. Cell Biol.* **221**, e202104046 (2021).
45. A. L. Bull *et al*., Actin dynamics as a multiscale integrator of cellular guidance cues. *Front. Cell Dev. Biol.* **10** (2022).
46. N. Ramakrishnan, P. Sunil Kumar, R. Radhakrishnan, Mesoscale computational studies of membrane bilayer remodeling by curvature-inducing proteins. *Phys. Rep.* **543**, 1–60 (2014).
47. R. K. Sadhu *et al*., Experimental and theoretical model for the origin of coiling of cellular protrusions around fibers. *Nat. Commun.* **14**, 5612 (2023).
48. R. K. Sadhu *et al*., A theoretical model of efficient phagocytosis driven by curved membrane proteins and active cytoskeleton forces. *Soft Matter* **19**, 31–43 (2023).
49. N. S. Gov, V. Kralj-Iglič, R. K. Sadhu, L. Mesarec, A. Iglič, "Chapter 25 - physical principles of cellular membrane shapes" in *Plasma Membrane Shaping* (Academic Press, 2023), pp. 393–413.
50. M. Drab *et al*., "Chapter 26 - modeling cellular shape changes in the presence of curved membrane proteins and active cytoskeletal forces" in *Plasma Membrane Shaping* (Academic Press, 2023), pp. 415–429.
51. T. Takenawa, H. Miki, WASP and WAVE family proteins: Key molecules for rapid rearrangement of cortical actin filaments and cell movement. *J. Cell Sci.* **114**, 1801–1809 (2001).
52. A. Y. Pollitt, R. H. Insall, WASP and SCAR/WAVE proteins: The drivers of actin assembly. *J. Cell Sci.* **122**, 2575–2578 (2009).
53. T. E. Stradal *et al*., Regulation of actin dynamics by wasp and wave family proteins. *Trends Cell Biol.* **14**, 303–311 (2004).
54. W. Helfrich, Elastic properties of lipid bilayers: Theory and possible experiments. *Zeitschrift Naturforschung C* **28**, 693–703 (1973).
55. D. Espriu, Triangulated random surfaces. *Phys. Lett. B* **194**, 271–276 (1987).
56. S. Penič, A. Iglič, I. Bivas, M. Fošnarič, Bending elasticity of vesicle membranes studied by Monte Carlo simulations of vesicle thermal shape fluctuations. *Soft Matter* **11**, 5004–5009 (2015).
57. J. Stites *et al*., Phosphorylation of the dictyostelium myosin ii heavy chain is necessary for maintaining cellular polarity and suppressing turning during chemotaxis. *Cell Motil. Cytoskeleton* **39**, 31–51 (1998).
58. N. Andrew, R. H. Insall, Chemotaxis in shallow gradients is mediated independently of ptdins 3-kinase by biased choices between random protrusions. *Nat. Cell Biol.* **9**, 193–200 (2007).
59. M. P. Neilson *et al*., Chemotaxis: A feedback-based computational model robustly predicts multiple aspects of real cell behaviour. *PLoS Biol.* **9**, e1000618 (2011).
60. M. Schröder, Master's thesis (Georg August University of Göttingen, 2018).
61. K. H. Song, J. Lee, H. R. Jung, H. Park, J. Doh, Turning behaviors of T cells climbing up ramp-like structures are regulated by myosin light chain kinase activity and lamellipodia formation. *Sci. Rep.* **7**, 1–10 (2017).
62. C. Guetta-Terrier *et al*., Protrusive waves guide 3D cell migration along nanofibers. *J. Cell Biol.* **211**, 683–701 (2015).
63. C. van der Putten, D. van den Broek, N. A. Kurniawan, Myofibroblast transdifferentiation of keratocytes results in slower migration and lower sensitivity to mesoscale curvatures. *Front. Cell Dev. Biol.* **10** (2022).
64. X. Yu *et al*., Biphasic curvature-dependence of cell migration inside microcylinders: persistent randomness versus directionality. bioRxiv (2022). https://www.biorxiv.org/content/10.1101/2022.12.30.522287v1 (Accessed 30 December 2022).
65. R. S. Fischer *et al*., Contractility, focal adhesion orientation, and stress fiber orientation drive cancer cell polarity and migration along wavy ecm substrates. *Proc. Natl. Acad. Sci. U.S.A.* **118**, e2021135118 (2021).
66. M. Riaz, M. Versaevel, D. Mohammed, K. Glinel, S. Gabriele, Persistence of fan-shaped keratocytes is a matrix-rigidity-dependent mechanism that requires $\alpha 5\beta 1$ integrin engagement. *Sci. Rep.* **6**, 34141 (2016).
67. T. Grevesse, M. Versaevel, G. Circelli, S. Desprez, S. Gabriele, A simple route to functionalize polyacrylamide hydrogels for the independent tuning of mechanotransduction cues. *Lab Chip* **13**, 777–780 (2013).
68. G. Bloomfield *et al*., Neurofibromin controls macropinocytosis and phagocytosis in *Dictyostelium*. *eLife* **4**, e04940 (2015).
69. S. Flemming, F. Font, S. Alonso, C. Beta, How cortical waves drive fission of motile cells. *Proc. Natl. Acad. Sci. U.S.A.* **117**, 6330–6338 (2020).
70. R. K. Sadhu, curvotaxis-codes. GitHub. https://github.com/rajsadhu3903/curvotaxis-codes. Deposited 14 April 2023.